JOURNAL OF CATALYSIS 57, 417–425 (1979)

Crystallite Size Distributions of Sintered Nickel Catalysts

J. T. RICHARDSON AND J. G. CRUMP

Department of Chemical Engineering, University of Houston, Houston, Texas 77004

Received April 24, 1978; revised November 24, 1978

Sintering of nickel on silica was followed by measuring the crystallite size distribution with a magnetic granulometry method. The initial distribution of a sample prepared by slow, homogeneous precipitation-deposition was very narrow but could be broadened by thermal treatment. The effects of temperature, time, initial distribution, and nickel concentration were studied.

The dispersion was very stable at 673 K but showed some broadening for sintering times up to 100 hr. Above 723 K, however, sintering occurred with the disappearance of small crystallites, reaching a limiting log-normal shape, independent of initial distribution or nickel concentration below 17 wt%. These results were interpreted as particle migration. The decline of surface area showed an order of 10 and an activation energy of 200 kJ/mole.

At temperatures approaching 873 K, the resulting distributions were bimodal, suggesting that the influence of pore-size distributions should be considered in sintering models.

INTRODUCTION

Sintering of dispersed metal catalysts results in irreversible deactivation and is an important problem in industrial catalysis. Catalyst formulations with refractory supports and spacers have been moderately successful in controlling excessive sintering. Further refinements in catalyst design are possible through the optimization of support texture and promoters. Success in these efforts depends upon an understanding of sintering mechanisms and their relationship to catalyst properties. Considerable theoretical progress has been made in recent years, resulting in descriptive models which are not necessarily competitive but merely applicable to different conditions. However, very little experimental verification has appeared. This paper describes changing crystallite size distributions in sintered nickel catalysts, leading to speculations on the prevailing growth mechanism.

Two dominant theories have emerged (*1*). In the interparticle transport model, growth of crystallites occurs through the accumulation of atomic or molecular material transported from smaller crystallites via the carrier surface or through the gas phase. The alternative crystallite migration model invokes particle movement over the surface, followed by collision and coalescence.

Interparticle transport has been viewed as a two-dimensional analog of the "coarsening" or "ripening" of precipitate particles. Extending this model to thin films, Chakroverty (*2*) predicted a critical radius, r^*, such that crystallites of radius $r > r^*$ grow in size and those with $r < r^*$ diminish. The distribution function $f(t, t)$ obeys a continuity equation with two solutions valid for either surface diffusion or interface transfer control. For both solutions, $f(r, t)$ is the product of a time-dependent factor and one depending on r

0021-9517/79/060417-09$02.00/0

(*4*). Plots of the normalized distribution function against r/r^* are time independent. Furthermore, in both cases $f(r, t)$ exists over a finite range of r/r^* above which $f(r, t) = 0$.

Wynblatt and Gjostein reviewed and modified Chakroverty's treatment and agreed with the essential conclusions (*3*). Their calculated distributions for diffusional and interfacial control were independent of initial distribution.

Flynn and Wanke (*4–6*) developed an alternate model for interparticle transport, similar to evaporation and condensation processes among liquid droplets of different sizes. Variation in equilibrium vapor pressure with radius leads to transport of material from small to larger droplets. Similarly, smaller crystallites equilibrate with a larger atom concentration, so that large crystallites grow at the expense of smaller ones. This model predicts a final distribution strongly dependent on the initial distribution. Distributions which are broad or bimodal sinter more rapidly than narrow, unisized distributions.

According to the migration model, crystallites migrate, collide, and coalesce. Migration is analogous to a two-dimensional random walk. Ruckenstein and Pulvermacher (*7–9*) developed a theory for binary collisions between migrating crystallites. Crystallite motion is slow compared to coalescence and diffusion controls the sintering rate. Ruckenstein and Pulvermacher computed crystallite size distributions for both homogeneous and nonhomogeneous surfaces. For a nonhomogeneous surface, an equilibrium size distribution is reached after a sufficiently long time and the metal surface area no longer decreases. Homogeneous surfaces result in a universal distribution, independent of initial distribution.

Granqvist and Buhrman (*10–13*), reexamining previous work on both interparticle transport and crystallite migration, concluded that the two theories predict distinctly different distributions, thus providing a means for identifying the sintering mechanism. The crystallite migration model predicts removal of very small crystallites with a distribution "tailing" on the high-diameter side of the peak. The interparticle transport model predicts a substantial tail on the low-diameter side. Wanke, however, argues that certain initial distributions give log-normal functions upon sintering via interparticle transport (*14*). The shape of the final distribution may not be sufficiently sensitive to the mechanism to serve as a diagnostic tool.

However, early changes in the distribution are significant. The interparticle transport model predicts a broadening of the distribution, at least initially, as smaller crystallites are generated to produce larger ones. The crystallite migration model, however, results in an increase of the average size with the disappearance of the small crystallites. These predictions must be modified if crystallite splitting occurs (*8*).

Wynblatt and Gjostein postulated that both sintering mechanisms contribute to sintering, their relative importance depending upon the average crystallite size (*1*). Since crystallite mobility decreases as size increases, migration dominates for small crystallites, while interparticle transport occurs for the larger ones.

Both models predict a loss of surface area, S, according to the kinetic rate law:

$$dS/dt = kS^n. \qquad (1)$$

The interparticle transport model gives values of n over a wide range, from <2 to >13. The crystallite migration model, assuming crystallite diffusion control, results in n between 4 and 8, with larger values possible for facetting (*1*).

Determinations of surface areas, with assumptions of constant adsorption stoichiometry and complete surface accessibility, may not be sufficient to distinguish between the two theories.

The history of the crystallite size distributions may be the only reasonable method for differentiating the two models. Most data have come from electron microscopy and are both scarce and uncertain. While resolution is high with transmission electron microscopy, major difficulties affect the measurements of small crystallites. Sampling errors may be serious and statistical errors significant even if many crystallites are measured. Focusing precision is questionable for small crystallites and the possibility of electron beam interaction always present (*15*).

Nevertheless, studies have been made in which size distributions point to a mechanism. Nakamura, for example, found the disappearance of small platinum crystallites on charcoal (*16*). Bett *et al.* used size distributions from electron micrographs to support crystallite migration (*17*).

Greater confidence in sintered distributions result if measurements are made *in situ* on the same sample. This is possible using a magnetic granulometry method (*18*). We have applied the method to the sintering of nickel on silica prepared with high but dispersed metal loading. Changes in distribution with time have been measured and the effect of temperature and initial distribution determined in an attempt to identify the prevailing mechanisms.

EXPERIMENTAL

Catalyst Preparation

The nickel–silica catalyst was prepared with a homogeneous precipitation-deposition method described in a previous paper (*19*). Slow nucleation of nickel ions on Cabosil support was achieved through the hydrolysis of urea at 363 K, resulting in very narrow and reproducible crystallite size distribution at high loadings (17 wt% nickel).

Magnetic Measurements and Calculations

The sample cell and magnetometer have been described earlier (*19*). The fresh catalyst was loaded into the cell and reduced at selected conditions. Magnetization curves were measured at 298 K for the fresh catalyst before and after sintering for various times and temperatures. The last step was determination of the saturation magnetization and degree of reduction after excessive sintering in helium at 1073 K.

Crystallite size distributions were calculated from magnetization data using developed procedures (*18*). Model calculations confirmed that this techniques is sufficiently sensitive to detect changes in distributions resulting from these treatments.

Catalyst Reduction and Sintering

A different sample was used for each temperature run. Each catalyst was reduced at 653 K in 60 cm^3/min of hydrogen for 15 hr so that 50 to 60% of the nickel was reduced. Complete reduction was possible by increasing the hydrogen flow in experiments designed to check the effect of reduced nickel concentration.

Following reduction and before magnetic measurement the chemisorbed hydrogen was removed in a helium stream at 673 K for 1 hr.

Sintering experiments were made in helium at 673, 723, 773, 823, and 873 K, with measurements at 1, 5, 15, and 30 hr. The run at 673 K was extended for 150 hr. After sintering at a specific temperature and time interval, the sample was cooled rapidly to ambient temperature, measured, and replaced rapidly in the hot furnace.

Due to slight differences in reduction procedures, initial distributions varied in width although centered at the same radius. They were close enough, however, that the starting points could be taken as equivalent. In a few cases, the catalyst

was presintered at a lower temperature. This allowed the effect of different thermal treatments, i.e., initial distribution, to be investigated.

RESULTS

Temperature Effects

Sintering results at 673, 773, and 873 K are given in Figs. 1, 2, and 3, respectively. Other temperatures are not shown since they show intermediate values with the same trends.

This preparation is very stable at 673 K. The mean radius is almost constant at 1.5 nm, but the distribution first broadens and then moves toward higher radii. Finally, after 150 hr, small crystallites disappear. At 773 K, the shift of the mean radius toward higher values is so pronounced that all crystallites below 1.5 nm are removed.

Sintering at 873 K was more dramatic. The original distribution was broader than usual but the growth of large crystallites at the expense of smaller ones is apparent, resulting in a stable bimodal distribution.

Figure 4 shows the decline of surface

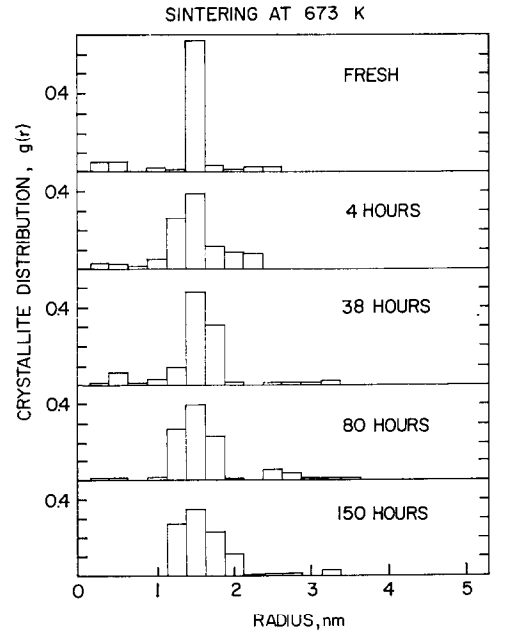

FIG. 1. Crystallite size distributions for sintering at 673 K.

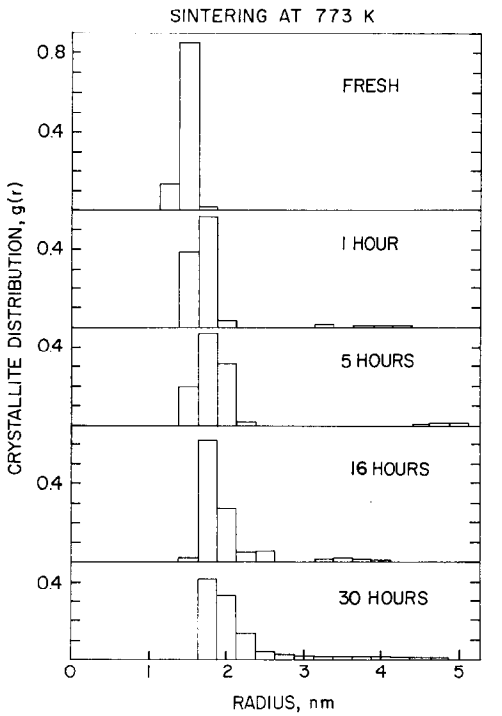

FIG. 2. Crystallite size distributions for sintering at 773 K.

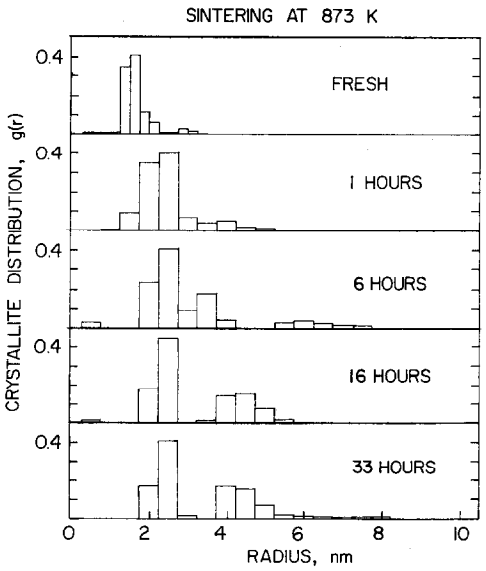

FIG. 3. Crystallite size distributions for sintering at 873 K.

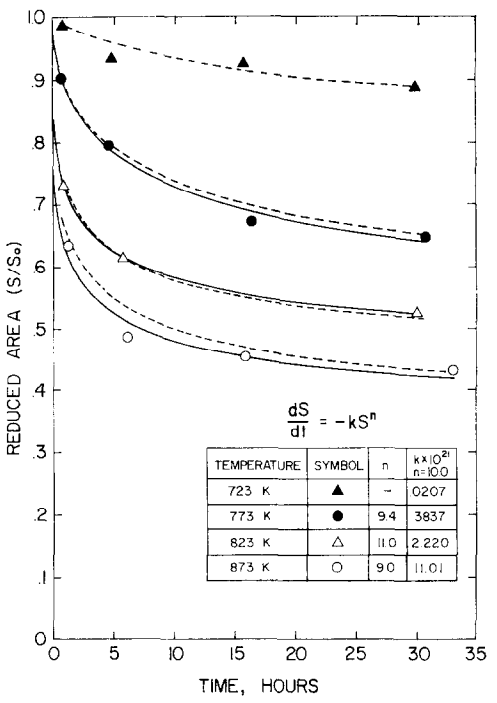

FIG. 4. Surface area decline for sintered samples.

area at various temperatures. These surface areas were calculated from the distributions. Free from the objections raised for experimental values, they should be a better test for the competing models.

The data in Fig. 4 were fitted to Eq. (1) by optimizing k and n for each temperature. Fitting of data below 723 K was not attempted since a broad range of n values gave equally good results. For 773, 823, and 873 K, however, good fits (solid lines) with n from 9 to 11 were found. Corresponding values of k were erratic and followed no trend. Assuming that n is constant, we set n equal to 10 and recalculated the value of k for each temperature. These are shown as the dashed curves in Fig. 4. The fit is acceptable, especially since the k values now increase with temperatures and follow an Arrhenius expression as shown in Fig. 5. The activation energy is 200 kJ/mole.

Effect of Initial Distribution

Sintering experiments were made with initial distributions varied by prior thermal treatment. For example, reduction at 673 K was followed by 30 hr of heating at 773 K, broadening the fresh distribution. This was then taken as the original distribution for sintering runs at 823 K.

Table 1 gives the nickel surface areas computed from the measured distributions for these experiments.

All samples originated from the same preparation (17 wt.% Ni). The results in Table 1 indicate the following: (i) Sintering at a given temperature is more rapid for higher initial distribution. Com-

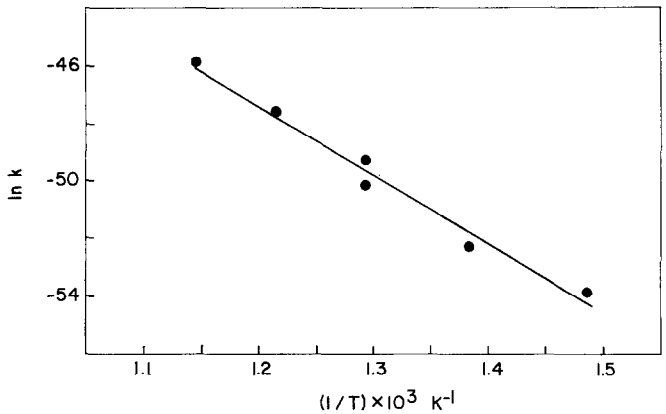

FIG. 5. Temperature dependence of k with $n = 10$.

TABLE 1

Nickel Surface Areas for Sintered Samples with Prior Thermal Treatments

	Surface Area $\times 10^{-5}$, m^2/kg Ni			
	A	B	C	D
Prior thermal treatment	none	150 hr, 673 K +30 hr, 723 K +30 hr, 773 K	30 hr, 723 K +30 hr, 773 K	30 hr, 773 K
Time of sintering at 822 K, hr				
0	2.07	1.43	1.42	1.27
1	1.52	1.40	1.36	—
5	1.27	1.34	1.21	1.10
15	—	1.13	1.12	0.95
30	1.09	1.05	1.05	0.91
$(S/S_0)_{30\ hr}$	0.53	0.73	0.74	0.72

pare, for example, Sample A with B, C, and D at 823 K and Sample D with B and C at 773 K. Samples B and C are almost identical since heating at 673 K has very little effect. (ii) Regardless of initial distributions, all samples appear to approach a limiting surface.

This last point was further examined by plotting a fit of Eq. (1) with $n = 10$ for Sample A and superimposing the other samples upon it (Fig. 6). For samples B and C, the initial surface area values were adjusted to the curve and the corresponding time added to the subsequent sintering times in Table 1. Both show relatively good agreement with the kinetic curve. For Sample D, the agreement is not so good. The best fit was obtained by adjusting the value at 5 hr to the curve. The distribution of this sample after prior treatment was bimodal, whereas the others were not. The significance of this, if any, is not clear at this time.

However, even with the scatter introduced by Sample D, the results in Fig. 6 suggest that narrow distributions sinter faster than broader ones along a common kinetic path to the same ultimate value that depends upon the temperature.

The Effect of High Temperature

Sintering at 873 K for 30 hr gave bimodal distributions, as shown in Fig. 7. The starting samples were C, D, and E (after the experiments reported in Table 1) and an untreated sample. Final surface areas were 0.74, 0.69, 0.68, and 0.80 $\times 10^5$ m^2/kg Ni, respectively. Final dispersions are again in the same range but crystallites about 2.0 nm in radius appear to be stabilized.

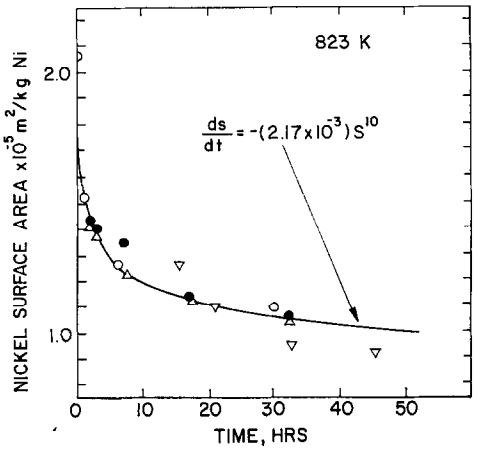

FIG. 6. Superimposed surface area decline curve for different initial distributions. ○ Sample A, ● Sample B, △ Sample C, ▽ Sample D.

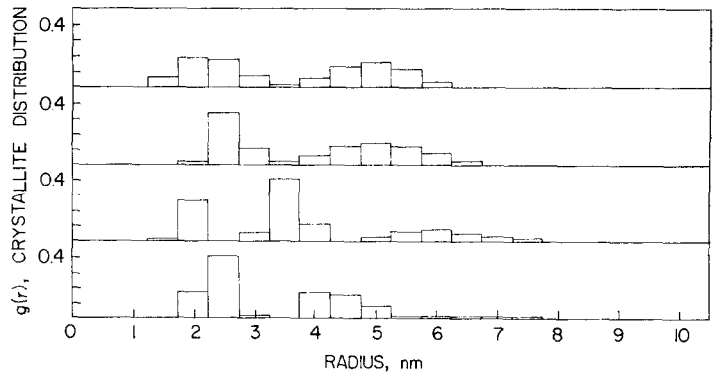

FIG. 7. Crystallite size distributions for sintering at 873 K. From top to bottom: Sample C, D, A, and no treatment.

Effect of Nickel Concentration

The degree of reduction of these catalysts is controllable without serious changes in the crystallite size distributions by means of the hydrogen flow rate (*19*). Accordingly, samples were prepared with 50 and 100% of the total nickel reduced, corresponding to 8.5 and 17 wt% nickel, respectively. The samples were sintered for 30 hr at 773 K.

Although the sintering rate increased slightly with concentration, the difference between S/S_0 for the 8 and 17 wt% of Ni samples was only 3–5%, less than the error in the data. However, for $n = 10$, a twofold increase in k of Eq. (1) results in but a 5% decrease in S/S_0 at 30 hr. Significant changes (about 15%) result only if k is increased by a factor of 10.

DISCUSSION

Sintering at 673 K produced very little change in the mean crystallite radius but the distribution appeared to broaden. This result is consistent with the interparticle transport mechanism. Usually this effect is expected at higher temperature where atom–crystallite detachment is favored. However, crystallite migration is also retarded at lower temperatures so that these observations may indicate a slight dominance of interparticle transport as the growth mechanism.

At higher temperatures, however, the weight of evidence favors the migration model. Specifically, in the temperature range 723 to 823 K the following evidence is significant:

(i) Progressive sintering leads to the disappearance of small particles as the distribution assumes a log-normal shape and moves to higher values.

(ii) A limiting distribution is approached, regardless of the shape of the initial distribution.

(iii) Total surface areas fit Eq. (1) with an order, n, fairly constant over the temperature range, and an activation energy of 200 kJ/mole. The value of 10 for n is within the predicted range for the migration model if adjustments are made for facetting. The sensitivity of k to metal concentration is low over the range studied.

An activation energy of 200 kJ/mole is so much smaller than the energy for atom detachment (431 kJ/mole from sublimation energies) that interparticle transport seems unlikely. Estimates of crystallite migration distances may be found from the expression (*1*):

$$X_c = 2(D_c t)^{\frac{1}{4}}, \qquad (2)$$

where X_c is the distance travelled in time t, and the crystallite diffusively is given by (*20*):

$$D_c = 0.301 D_s (a/r)^4 \qquad (3)$$

in which a is the atomic diameter and r the crystallite radius. The value of D_s, the metal surface diffusively, is found from (*21*):

$$D_s = D_0 \exp(-Q/RT), \qquad (4)$$

where D_0 is a constant and Q the activation energy for surface diffusion. Equation 4 is for nonfacetted spheres. Facetted polyhedra give D_s values a factor of 10^4 lower.

For nickel, with $D_0 = 300$ cm²/sec, $Q = 159$ kJ/mole, $a = 0.23$ nm, equations (2)–(4) give the results reported in Table 2.

A 2-nm-radius crystallite migrates about 175 crystallite diameters in 1 hr, with sufficient chances for collisions to occur. With facetting, this distance is reduced to about two diameters and the system is fairly stable.

At 873 K the distance increases to about ten diameters and faster sintering occurs. These points are qualitatively confirmed in Figs. 2 and 3 where, at the lower temperature, growth occurs mostly at the expense of the smaller crystallites. Predicted distances may be too small to account for the observed rates, but the overall behavior indicates facetting with migration as the most probable mode.

Caution must be exercised, however, in applying these principles to this catalyst system. The ideal model of a sphere moving across an infinite plane is not applicable to nickel catalysts with high loadings. The measured BET surface area of the fresh catalyst is 2.91×10^5 m²/kg, indicating nickel silicate microparticles of about 3.0-nm radius (*22*). These form a matrix with a broad pore-size distribution above 0.5-nm radius. Behavior of metal crystallites in this pore system is not expected to conform to the existing models.

TABLE 2

Migration Distances for Nickel Crystallites[a]

Radius, nm	Distance X_c, nm (without faceting)
1.0	3×10^3
2.0	7×10^2
3.0	3×10^2
5.0	10^2
10.0	3×10

[a] Temperature = 773 K, time = 1.0 hr.

Wynblatt and Gjostein (*1*) suggested that crystallites with dimensions close to those of the pore are stabilized against sintering. This may indeed account for the observations here and also for bimodal distributions at higher temperature. Similar bimodal crystallite size distributions are also found in commercial catalysts (*18*) where pore-related mechanisms may also be applicable. Speculation on the role of texture in sintering must be deferred until appropriate refinement of existing models are made. In the meantime, we are gathering data on the relationship between metal crystallite sintering and pore texture. These will be reported at a later date.

CONCLUSIONS

Nickel on silica catalysts prepared by the homogeneous precipitation method are stable against sintering at reduction temperatures. As the temperature increases, crystallite growth occurs via crystallite migration so that a limiting distribution is attained. Surface area decline follows a power rate law with a constant order of 10 and an activation energy of 200 kJ/mole. Pore size distribution, however, may be important in the process and account for bimodal distribution at high temperatures.

ACKNOWLEDGMENT

The authors thank the National Science Foundation for support of this work through Grant No. ENG76-10071.

REFERENCES

1. Wynblatt, P., and Gjostein, N. A., *Prog. Solid State Chem.* **9**, 21 (1975).
2. Chakraverty, B. K., *J. Phys. Chem. Solids* **28**, 2401 (1967).
3. Wynblatt, P., and Gjostein, N. A., *Script Met.* **7**, 969 (1973).
4. Flynn, P. C., and Wanke, S. E., *J. Catal.* **34**, 300 (1974).
5. Flynn, P. C., and Wanke, S. E., *J. Catal.* **34**, 390 (1974).
6. Flynn, P. C., and Wanke, S. E., *J. Catal.* **37**, 432 (1974).
7. Ruckenstein, E., and Pulvermacher, B., *AIChE J.* **19**, 356 (1973).
8. Ruckenstein, E., and Pulvermacher, B., *J. Catal.* **29**, 224 (1973).
9. Ruckenstein, E., and Pulvermacher, B., *J. Catal.* **35**, 115 (1974).
10. Granqvist, C. G., and Buhrman, R. A., *J. Appl. Phys.* **27**, 693 (1975).
11. Granqvist, C. G., and Buhrman, R. A., *Solid State Commun.* **17**, 123 (1976).
12. Granqvist, C. G., and Buhrman, R. A., *J. App. Phys.* **47**, 2200 (1976).
13. Granqvist, C. G., and Buhrman, R. A., *J. Catal.* **46**, 238 (1977).
14. Wanke, S. E., *J. Catal.* **46**, 234 (1977).
15. Flynn, P. C., and Wanke, S. E., *Catal. Rev.* **12**, 93 (1975).
16. Nakamura, M., *J. Catal.* **39**, 125 (1975).
17. Bett, J. A., Kinoshita, K., and Stonehart, P., *J. Catal.* **35**, 307 (1974).
18. Richardson, J. T., and Desai, P., *J. Catal.* **42**, 294 (1976).
19. Richardson, J. T., and Dubus, R. J., *J. Catal.* **54**, 207 (1978).
20. Maat, H. J., and Moscu, L., *in* "Proceedings of the Third International Congress on Catalysis," Vol. II, p. 1277. North–Holland, Amsterdam, 1965.
21. Somorjai, G., "Principles of Surface Chemistry," p. 114. Prentice–Hall, New York, 1976.
22. Richardson, J. T., Dubus, R. J., Crump, J. G., Desai, P., Osterwalder, U., and Cale, T. S., *in* "Preparation of Catalysts" (B. Delmon, P. Grange, P. Jacobs, and G. Poncelet, Eds.). Elsevier, Amsterdam, 1979.